16th World Conference on Earthquake, 16WCEE 2017
Santiago Chile, January 9th to 13th 2017
Paper N° 2407
Registration Code: S-A1463505141

# EVALUATING THE DYNAMIC PROPERTIES OF THE MATERIAL SKELETON OF LIQUEFIABLE SANDS AT LOW CONFINING PRESSURES

Y. Wang[(1)], A.K. Keene[(2)], and K.H. Stokoe, II[(3)]

[(1)] *Graduate Research Assistant, Civil, Architectural, and Environmental Engineering Department, University of Texas at Austin, USA, yaningwang11@gmail.com*
[(2)] *Graduate Research Assistant, Civil, Architectural, and Environmental Engineering Department, University of Texas at Austin, USA, akkeene@utexas.edu*
[(3)] *Professor, Jennie C. and Milton T. Graves Chair in Engineering, Civil, Architectural, and Environmental Engineering Department, University of Texas at Austin, USA, k.stokoe@mail.utexas.edu*

## *Abstract*

A next-generation, combined resonant column and torsional shear (RCTS) system has been developed to measure the cyclic and dynamic properties of all types of soils with high resolution, increased accuracy, and no complications from system compliance. In this study, the dynamic properties of the material skeleton of liquefiable sands from Christchurch, NZ, were evaluated at low, effective isotropic confining pressures, $\sigma_0$' < 60 kPa. Bulk samples of poorly-graded fine sand were collected from one site and were transported to the University of Texas. Specimens were reconstituted in unsaturated, loose and medium-dense states for dynamic testing. The small-strain properties ($V_S$ – log $\sigma_0$', $G_{max}$ – log $\sigma_0$' and D – log $\sigma_0$') and the nonlinear properties (G – log $\gamma$, $G/G_{max}$ – log $\gamma$, and D – log $\gamma$) were determined at confining pressures of 14, 28, and 55 kPa. Shear strains in these tests ranged over about 4.5 orders of magnitude (from $10^{-5}$ % to 0.2%). The small-strain log $V_S$ – log $\sigma_0$' relationships are in good agreement with field $V_S$ – depth profiles. The expected in-situ $G/G_{max}$ – log $\gamma$ relationship for saturated sand during earthquake shaking is calculated using $G/G_{max}$ values of unsaturated specimens in the laboratory and pore water pressures measured in the field at corresponding strains.

*Keywords: shear modulus; material damping; liquefiable sand; torsional resonant column; pore pressure generation*

## 1. Introduction

In 2010-2011, the city of Christchurch, NZ, and the surrounding suburbs experienced widespread liquefaction multiple times during a series of powerful earthquakes known as the Canterbury earthquake sequence. The sand tested in this study is from one site in a suburb of Christchurch named Bexley. The sand was recovered as part of a comprehensive field study to determine the effectiveness of shallow (depth ~ 4 m) ground improvements to inhibit liquefaction triggering in future earthquakes by Van Ballegooy et al. (2017) [1]. The sand was recovered as disturbed samples from depths of 2 and 3 m in the zone where liquefaction occurred multiple times. The sand was recovered by a significant effort that involved dewatering, trenching, logging and sampling at the end of the ground-improvement study [1].

Combined resonant column and torsional shear (RCTS) equipment was employed to measure the deformational characteristics of reconstituted sand specimens, with a focus on modulus and material damping in shear. Development and upgrades of RCTS equipment, testing procedures and cyclic/dynamic material property databases have been continually pursued at The University of Texas at Austin over the past four decades. With RCTS equipment, both resonant column (RC) and torsional shear (TS) tests can be performed in a sequential series on the same specimen over shear strains ($\gamma$) ranging from about $10^{-6}$ % to slightly more than $10^{-1}$ %. In this study, only the RC portion of the RCTS device was employed to evaluate the dynamic properties of liquefiable sand specimens over confining stresses ranging from 14 to 441 kPa. The sand specimens were unsaturated and were reconstituted in loose and medium-dense states. The small-strain dynamic properties of the sand were determined at $\gamma$ ~ 0.0006%. The small-strain properties are presented in terms of shear wave velocity, $V_S$, shear modulus, $G_{max}$, and material damping ratio in shear, $D_{min}$. The variations in these properties with mean effective confining pressure, $\sigma_0$', are presented on log-log scales which results in the formation of linear or bi-linear relationships. The small-strain shear wave velocities obtained from RCTS tests are also compared with values

determined in previous laboratory studies and with in-situ shear wave velocities determined from crosshole testing at the Bexley site.

Nonlinear dynamic tests of the sand specimens were conducted at strains from the elastic threshold strain ($\gamma_t^e$) to moderately-large shear strains of 0.1 to 0.2%. These measurements were used to develop relationships between shear modulus and $\gamma$ (G – log $\gamma$), normalized shear modulus and $\gamma$ ($G/G_{max}$ – log $\gamma$) and material damping ratio in shear and $\gamma$ (D – log $\gamma$). Modified hyperbolic equations were fit to the nonlinear relationships to model the strain-dependent, nonlinear dynamic behavior of the material skeleton. During earthquake shaking, the $G/G_{max}$ – log $\gamma$ and D – log $\gamma$ relationships of the sand would differ if the sand were saturated. The main difference is the generation of excess pore pressure leading to liquefaction which reduces the effective stress. As an example, changes to the $G/G_{max}$ – log $\gamma$ curve are presented based on strain-dependent, excess pore water pressure generation that was measured in field shaking tests by Stokoe et al. (2014) [2].

## 2. Dynamic Testing Method

The computer-controlled RCTS system used in this study can be idealized as a fixed-free system. The bottom end of the specimen is fixed against rotation at the base pedestal and top end of the specimen is connected to a freely-rotating, electro-magnetic drive system (see Fig. 1). The coil-magnet drive system, which consists of a top cap and drive plate with permanent magnets, rotates freely to excite the specimen in slow cyclic (TS) or dynamic (RC) torsional motion.

The basic operational principle of RC testing is to vibrate a cylindrical specimen, with a height-to-diameter ratio of between about 2.0 to 2.5, in first-mode, torsional resonant motion. Sinusoidal torsional excitation is applied to the top of the specimen over a range of frequencies. The variation of the shear strain amplitude of the specimen with frequency is determined using both an accelerometer and a pair of proximitors to measure torsional motion. Once first-mode resonance is established, the resonant frequency and maximum amplitude of vibration are calculated. These measurements are then combined with equipment characteristics and geometry of the specimen to calculate shear wave velocity and shear modulus based on elastic wave propagation theory as discussed in Richart, Hall and Woods (1970) [3]. Material damping (D) is determined either from the width of the frequency response curve at small strains where D is independent of $\gamma$ or from the free-vibration decay curve at small strains and at larger strains where D varies with $\gamma$.

The TS test is another testing method for determining shear modulus and material damping. In TS testing, the same equipment configuration is used, but it is operated in a different manner. A cyclic torsional force with a given frequency, generally below 3 Hz, is applied at the top of the specimen. Instead of determining the resonant frequency, the stress-strain hysteresis loop is determined from measuring the torque-twist response of the specimen. Proximitors are used to measure the angle of twist, while the voltage applied to the coil is calibrated to determine the applied torque. Shear modulus is calculated from the slope of a line through the end points of the hysteresis loop, and material damping is obtained from the area of the hysteresis loop (i.e., the amount of energy dissipated in one cycle).

The next-generation computer-controlled RCTS system used herein can be divided into four basic subsystems. These subsystems are: (1) a pneumatic confinement system that applies isotropic confining pressure to the specimen, (2) a drive system that is used to apply sinusoidal torsional excitation at the top of the specimen, (3) a height monitoring system that is used to measure the height-change of the specimen during confinement, and (4) a motion monitoring system that is used to measure the torsional response at the top of the specimen. The confinement system is operated manually while the other three systems are controlled by a next-generation, automated computer system with automated data acquisition and data processing. The combined RCTS equipment is calibrated annually to assure proper maintenance and accurate measurement during operation.

The RCTS control system is composed of a National Instrument PXI 1033 Chassis with 16-channel (PXI 6251) and 4-channel (PXI 4461) boards that provide excitation to the RCTS drive system and to the active sensors and also acquire outputs from the sensors. The PXI 4461 is a 24-bit system with 6 adjustable voltage ranges, which are ± 0.316, 1.00, 3.16, 10.0, 31.6, 42.4 volts. When the lowest voltage range is selected, the PXI 4461 has a minimum voltage resolution of $4.30\times10^{-8}$ V. The use of this control system for RC and TS testing

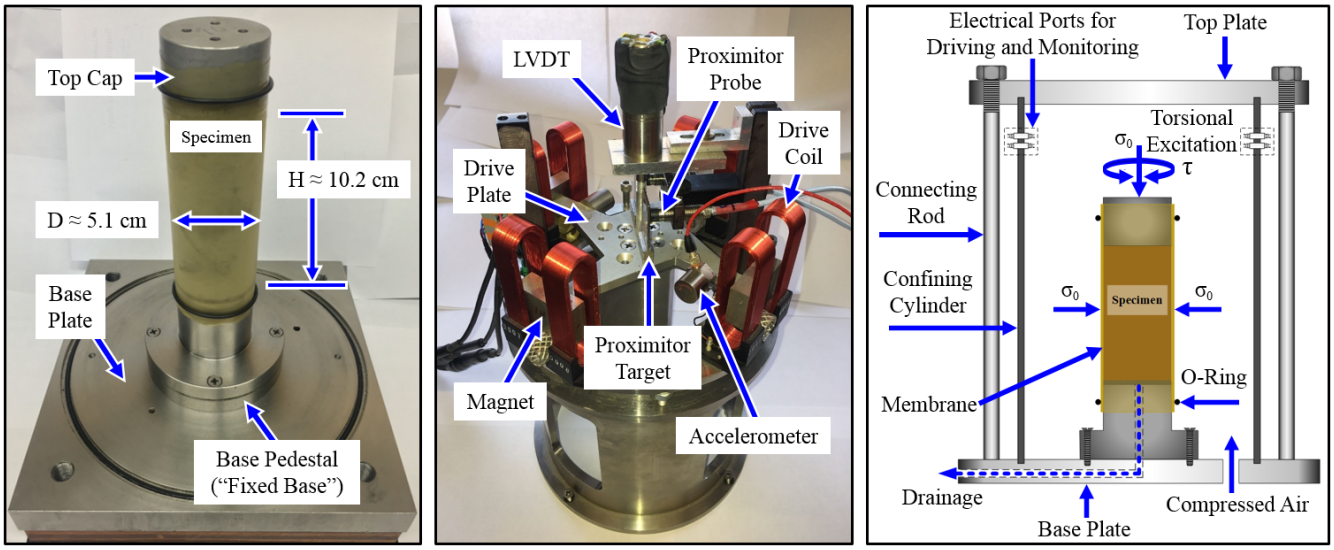


(a) Reconstituted sand specimen on base pedestal and confined using a vacuum

(b) Driving and monitoring systems on support cylinder

(c) Simplified schematic of RCTS confining system (driving system not shown)

Fig. 1 – Reconstituted sand specimen (a), photographs of the coil-magnet drive system and accelerometer, proximitor and LVDT monitoring system (b) and simplified schematic of RCTS confining system (c)

requires a thorough understanding of the capabilities of the testing system and the use of computerized subroutines, developed in National Instruments LabVIEW, for operating the equipment and processing the data. The features of the testing system comprise a number of custom, build-in improvements in resolution, maximum and minimum analog outputs, and reduction of the system noise floor (Keene, 2017) [4]. The testing system resolution and the build-in improvements, in combination with the computerized subroutines that digitally process and analyze signals from the sensors, has led to shearing strain measurements in the resonant column as low as $10^{-7}$ %. Thus, the dynamic properties of liquefiable sands at low confining pressures, from the linear to significantly-nonlinear shear strain ranges, have been obtained. The parameters obtained from RCTS tests generally include shear strain ($\gamma$), shear wave velocity ($V_S$), shear modulus (G), material damping ratio (D) and estimated void ratio (e) during time of confinement at each pressure.

## 3. Soil Tested

The liquefiable sand from Christchurch was recovered as bag samples from depths of 2 and 3 m by dewatering and trenching. The specimen designations used herein are S6(2m) and S6(3m). Sieve analyses (ASTM D6913-04, 2009) [5] were performed on each sample to determine grain-size distributions. The values of percent passing for the various particle diameters, D, are presented in Table 1. The uniformity coefficient, $C_u$ (= $D_{60}$ /$D_{10}$), was then determined. Values of $C_u$ are 1.81 and 1.55 for S6(2m) and S6(3m), respectively, as presented in Table 1. Based on the Unified Soil Classification System (USCS) (ASTM D2487-11, 2011) [6], the liquefiable sand from Site 6 classifies as poorly graded sand (SP). The sand is fine sand with fines content (FC) less than 3%. The specific gravity of the sand particles is assumed to be 2.65. Using the estimated Roundness (R = (minimum radius of the particle edges) / (inscribed radius of the entire particle)) and $C_u$, values of minimum void ratio, $e_{min}$, and maximum void ratio, $e_{max}$, were estimated from Youd (1973) [7]. The $e_{min}$ and $e_{max}$ values were also estimated from Menq (2003) [8]. The values of $e_{min}$ and $e_{max}$ determined using each method are presented in Table 1.

Each sand specimen was reconstituted as a cylindrical specimen with a diameter of about 5.1 cm and a height of about 10.2 cm, as shown in Fig. 1a. The under-compaction method (Ladd, 1978) [9] was used to build each specimen to a target uniform density. All specimens were compacted as moist sand, with a degree of saturation of about 20%. For the sand from each depth, target relative densities were 40% for the looser specimen and 80% for the denser one.

Table 1 – Grain size information of the liquefiable sand from Site 6 in Christchurch, NZ

| Site | Depth (m) | Fines Content (%) | $D_{10}$ | $D_{30}$ | $D_{50}$ | $D_{60}$ | $D_{95}$ | $C_u$ | Estimation[1] | | Estimation[2] | |
|---|---|---|---|---|---|---|---|---|---|---|---|---|
| | | | (mm) | | | | | | $e_{min}$ | $e_{max}$ | $e_{min}$ | $e_{max}$ |
| S6(2m) | 2.0 | 2.7 | 0.114 | 0.162 | 0.192 | 0.206 | 0.295 | 1.81 | 0.49 | 0.95 | 0.55 | 0.95 |
| S6(3m) | 3.0 | 2.6 | 0.128 | 0.164 | 0.186 | 0.198 | 0.250 | 1.55 | 0.52 | 1.00 | 0.61 | 1.04 |

Notes: 1. Based on Youd (1973) [7]. 2. Based on Menq (2003) [8].

## 4. Small-Strain Dynamic Properties Determined in the Laboratory

Small-strain tests using the resonant column device were performed to determine the dynamic properties of each sand specimen in the small-strain range, $\gamma \sim 0.0006\%$. These tests were performed at the following six isotropic confining pressures ($\sigma_0$): 14, 28, 55, 110, 221 and 441 kPa. At each confining pressure, RC testing was performed over a period of about 60 minutes. Since the specimens were drained during testing, $\sigma_0$ is estimated to equal the effective isotropic confining pressure, $\sigma_0$'; hence, any negative capillary stresses were assumed to be small. The variations of shear wave velocity ($V_S$), shear modulus ($G_{max}$) and material damping ratio ($D_{min}$) with isotropic confining pressure are discussed below. Only results from the S6(2m) specimens are presented graphically because they also well represent the results from S6(3m) specimens.

As shown in previous studies, $V_S$ and $G_{max}$ of all soils increase with $\sigma_0$'. In this study, the variations in $V_S$ and $G_{max}$ with $\sigma_0$' from RC testing of the looser and denser sand specimens are shown in Figs. 2a and 2b, respectively. The first point readily observed is that the denser specimen is stiffer (has larger $V_S$ and $G_{max}$ values at all $\sigma_0$'s) than the looser specimen. The second point is that the log $V_S$ – log $\sigma_0$' and log $G_{max}$ – log $\sigma_0$' relationships are well represented either by a single linear relationship for the denser specimen or by a bi-linear relationship for the looser specimen, with the first line having a "flatter slope" in the bi-linear relationship. The single linear relationships of the denser specimen indicate that the denser specimen was exhibiting a behavior similar to a normally consolidated (NC) specimen. On the other hand, the bi-linear log $V_S$ – log $\sigma_0$' and log $G_{max}$ – log $\sigma_0$' relationships indicate that the looser specimen was behaving like an overconsolidated (OC) specimen at lower pressures and then becoming normally consolidated at higher pressures. The equations that can be used to represent each linear segment in the log $V_S$ – log $\sigma_0$' and log $G_{max}$ – log $\sigma_0$' relationships are:

$$V_S = A_S(\sigma_0'/P_a)^{n_S} \quad \text{and} \tag{1}$$

$$G_{max} = A_G(\sigma_0'/P_a)^{n_G} \tag{2}$$

where $A_S$ is the value of $V_S$ at $\sigma_0$' = 101.3 kPa, $A_G$ is the value of $G_{max}$ at $\sigma_0$' = 101.3 kPa, $n_G$ and $n_S$ are the exponents of normalized pressure ($\sigma_0'/P_a$), and $P_a$ = 101.3 kPa (1 atm). Each linear segment of the log $V_S$ – log $\sigma_0$' and log $G_{max}$ – log $\sigma_0$' relationships for all specimens has been "best-fit" with Eqs. (1) and (2) using a least-squares regression method. The resulting values of the parameters ($A_S$, $n_S$, $A_G$ and $n_G$) are presented in Table 2. As seen in the table, the denser specimen from a depth of 3 m also shows an OC portion which, in this case, is only in the range around the lowest pressure of 14 kPa.

Void ratio (e) has a well known influence on $V_S$ and $G_{max}$, with denser soils forming stiffer skeletons at the same $\sigma_0$'. In terms of average values of $A_S$ for specimens from 2 and 3 m with similar densities, the average $A_{S,looser}$ is 209 m/s and the average $A_{S,denser}$ is 240 m/s. The square root of the void-ratio function F(e) ($1/(0.3 + 0.7e^2)$) (Hardin, 1978) [10] accounts for most of the difference between $A_{S,looser}$ and $A_{S,denser}$. The values of $A_S$ divided by the square root of F(e) are 180 and 182 m/s for the looser and denser specimens, respectively, at $\sigma_0$' = 1 atm. In terms of average values of $A_G$, average $A_{G,looser}$ is 68 MPa and average $A_{G,denser}$ is 98 MPa. Values of $A_G$ divided by F(e) are 50.5 and 56.6 MPa for the looser and denser specimens, respectively, at $\sigma_0$' = 1 atm. The F(e) function accounts for a significant portion of the difference between $A_{G,looser}$ and $A_{G,denser}$. However, some of the difference also occurs because the total unit weight of the sand ($\gamma_t$) enters the calculation of shear modulus ($G = (\gamma_t/g)V_S^2$); hence, the difference in the total unit weights creates about an 7.9% increase in $G_{max}$ of the denser sand. A factor not accounted for, different soil fabrics for loose and dense states, seems unimportant.

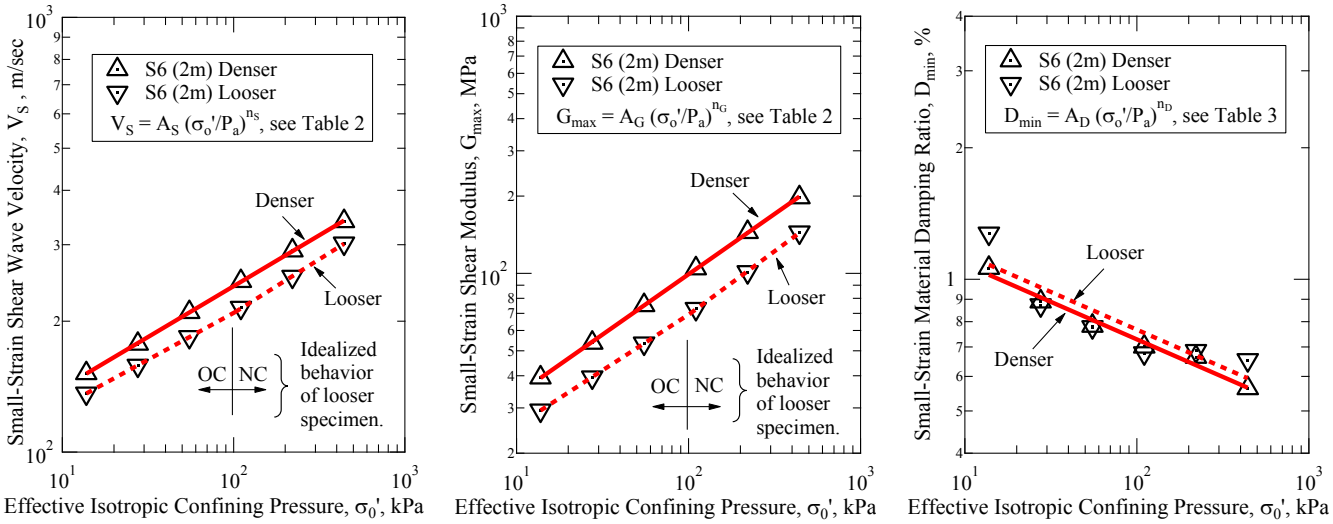


(a) Small-strain shear wave velocity, Vs (b) Small-strain shear modulus, $G_{max}$ (c) Small-strain material damping, $D_{min}$

Fig. 2 – Variations in small-strain shear wave velocity (a), shear modulus (b) and material damping (c) with effective isotropic confining pressure ($\sigma_0$') of two reconstituted specimens of sand from a depth of 2 m

Table 2 – Parameters fit to each linear segment of the log $V_s$ – log $\sigma_0$' and log $G_{max}$ – log $\sigma_0$' relationships from resonant column testing of reconstituted specimens of sand from depths of 2 and 3 m at Site 6

| Sample ID. | Est. Initial $D_r$[1], % | $\gamma_t$[2], g/cm$^3$ | Void Ratio, e, at $\sigma_0$' = 28 kPa | 110 kPa | 441 kPa | Water Content w, % | Idealized Consol. State[3] | $V_S$[4] $A_s$ (m/s) | $n_s$ | $G_{max}$[4] $A_G$ (MPa) | $n_G$ |
|---|---|---|---|---|---|---|---|---|---|---|---|
| S6 (2m) Looser | 37 | 1.58 | 0.789 | 0.786 | 0.779 | 6.6 | OC | 210 | 0.216 | 70 | 0.434 |
| | | | | | | | NC | 210 | 0.246 | 70 | 0.494 |
| S6 (2m) Denser | 77 | 1.71 | 0.621 | 0.619 | 0.614 | 4.5 | NC | 242 | 0.234 | 100 | 0.469 |
| S6 (3m) Looser | 48 | 1.57 | 0.799 | 0.795 | 0.785 | 6.4 | OC | 194 | 0.171 | 57 | 0.347 |
| | | | | | | | NC | 209 | 0.251 | 66 | 0.505 |
| S6 (3m) Denser | 84 | 1.69 | 0.639 | 0.637 | 0.631 | 4.2 | OC | 223 | 0.181 | 84 | 0.365 |
| | | | | | | | NC | 238 | 0.234 | 95 | 0.470 |

Notes:
1. $D_r = (e_{max} - e)/(e_{max} - e_{min}) \times 100\%$; and $e_{max}$ and $e_{min}$ are average values estimated from Youd (1973) [7] and Menq (2003) [8] in Table 1,
2. Estimated sand total unit weight, $\gamma_t$, at $\sigma_0$' = 1 atm,
3. OC = overconsolidated state, and NC = normally consolidated state,
4. $V_S = A_s(\sigma_0'/P_a)^{n_s}$, $G_{max} = A_G(\sigma_0'/P_a)^{n_G}$ and $P_a$ = 1 atm.

Finally, void ratio has another effect on the dynamic properties. For the same increment of $\sigma_0$', looser specimens have slightly larger changes in e, $V_S$ and $G_{max}$ than denser specimens because looser soil skeletons densify slightly more with increasing confining pressure. In terms of average values of $n_s$ and $n_G$ for similar-density specimens from 2 and 3 m, the average $n_{s,looser}$ is 0.249 and the average $n_{s,denser}$ is 0.234, while the average $n_{G,looser}$ is 0.500 and the average $n_{G,denser}$ is 0.470. These comparisons are only for the NC portion of the relationships because the overconsolidated portion was caused by the compaction effect and is assumed not to relate to the in-situ condition in Christchurch. The average values of e at $\sigma_0$' equal to one atmosphere are 0.80 and 0.63 for looser and denser specimens, respectively. For all sand specimens, the value of e of any specimen changed less than 1.8% during the 1-hour period at each pressure. Also, the value of e of any specimen changed by less than 2% over $\sigma_0$' increasing from 14 to 441 kPa.

Table 3 – Parameters fit to the log $D_{min}$ – log $\sigma_0$' relationships from resonant column testing of sand specimens from depths of 2 and 3 m at Site 6

| Sample ID. | Estimated Initial $D_r$[1], % | Void Ratio, e, at $\sigma_0$' = | | | $D_{min}$[2] | |
|---|---|---|---|---|---|---|
| | | 28 kPa | 110 kPa | 441 kPa | $A_D$ (%) | $n_D$ |
| S6 (2m) Looser | 37 | 0.789 | 0.786 | 0.779 | 0.77 | -0.17 |
| S6 (2m) Denser | 77 | 0.621 | 0.619 | 0.614 | 0.73 | -0.17 |
| S6 (3m) Looser | 48 | 0.799 | 0.795 | 0.785 | 0.82 | -0.18 |
| S6 (3m) Denser | 84 | 0.639 | 0.637 | 0.631 | 0.67 | -0.13 |

Notes: 1. $D_r = (e_{max} - e)/(e_{max} - e_{min}) \times 100\%$; and $e_{max}$ and $e_{min}$ are average values estimated from Youd (1973) [7] and Menq (2003) [8],
2. $D_{min} = A_D(\sigma_0'/P_a)^{n_D}$, $P_a$ = one atmosphere

Values of small-strain material damping ratio ($D_{min}$) of the looser and denser specimens from a depth of 2 m decrease with increasing $\sigma_0$' as shown in Fig. 2c. The first point observed is that the trend for the variation of $D_{min}$ with $\sigma_0$' is less well defined (shows more variability) than the $V_S$ and $G_{max}$ relationships. The second point is that looser specimens generally have slightly larger $D_{min}$ values at each $\sigma_0$' than the denser specimens. Some variability in the $D_{min}$ measurements is caused by ambient background noise, especially at $\gamma < 10^{-4}$ %. Therefore, each log $D_{min}$ – log $\sigma_0$' relationship is represented by a single linear relationship for convenience as:

$$D_{min} = A_D(\sigma_0'/P_a)^{n_D} \quad (3)$$

in which $A_D$ is the value of $D_{min}$ at $\sigma_0$' = 101.3 kPa, $n_D$ is the exponent of normalized pressure ($\sigma_0'/P_a$) and $P_a$ = 101.3 kPa. Each log $D_{min}$ – log $\sigma_0$' relationship has been "best-fit" with Eq. (3). The resulting values of parameters ($A_D$ and $n_D$) are presented in Table 3. In terms of average values, the values of $A_D$ are 0.80% and 0.70% for the looser and denser specimens, respectively, and the values of $n_D$ are -0.18 and -0.15, respectively. In general, values for $n_D$ are rather insensitive to void ratio for granular soils.

## 5. Comparison of Log $G_{max}$ – Log $\sigma_0$' Relationships from This and Earlier Studies

Earlier studies of the dynamic properties of sandy soils that have liquefied in previous earthquakes have been performed at The University of Texas by Kuo (1982) [13] and Haag (1985) [14]. All specimens tested in the earlier studies were recovered from Imperial Valley, California and were intact samples. Intact specimens were hand carved from these samples and were tested in a similar but earlier version of the RC equipment. Log $G_{max}$ – log $\sigma_0$' relationships from these earlier studies are compared with the same relationships for the S6(2m) – and S6(3m) – specimens in Fig. 3. Characteristics of the specimens in the earlier RC tests are given in the table embedded in the lower part of Fig. 3. The void ratios of the earlier specimens are all lower than the void ratios of the loose S6(2m) – and S6(3m) – specimens; hence, they are denser. However, the earlier specimens also have more fines than the specimens from Christchurch as indicated by their USCS classifications of SP-SM and SM. The increase in fines lowers the $V_S$ values and counteracts the decrease in void ratio. Thus, the earlier results compare very favorably with the $G_{max}$ values of the loose SP materials tested in this study.

## 6. Comparison of Field and Laboratory $V_S$ Values at Site 6

Shear wave velocities measured in the laboratory by RC testing can be compared with $V_S$ profiles determined in the field because crosshole seismic testing was performed at Site 6. Field testing was performed at two locations, designated as NS#1a and NS#1b (Stokoe et al. 2014) [2], that are very close to the location where the laboratory samples were obtained. The field $V_S$ measurements began at a depth slightly above the water table (depth ~ 0.5 m) and extended to a depth of 4.8 m. Profiles of $V_S$ calculated from the RC results are compared with the field $V_S$ measurements in the liquefiable sand in Fig. 4. The mean, in-situ confining pressure was calculated assuming $K_0$' (at-rest earth pressure coefficient) was equal to 0.5. The laboratory $V_S$ profiles of the sand in the loose ($D_r$ ~ 40%), medium ($D_r$ ~ 60%) and medium-dense states ($D_r$ ~ 80%) were calculated using Eq. (1) with $A_S$ and $n_S$ values determined using the F(e) function (Hardin, 1978) [10] and values presented in Table 2.

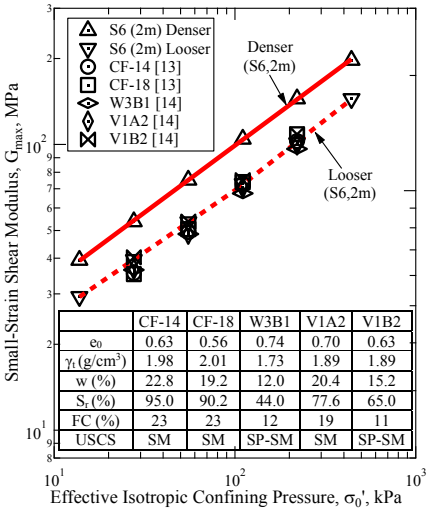


Fig. 3 – Comparison of laboratory log $G_{max}$ – log $\sigma_0$' relationships from this and earlier studies

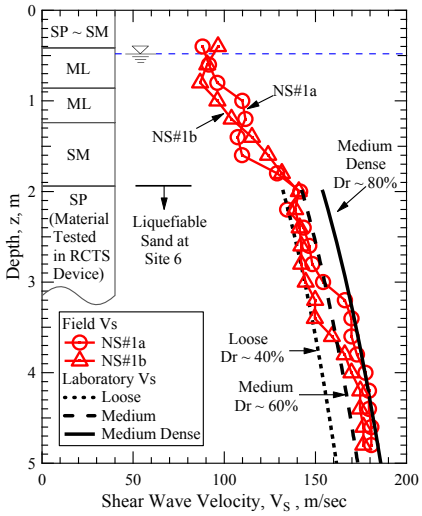


Fig. 4 – Comparison of $V_S$ values from field and lab measurements of liquefiable sand at Site 6

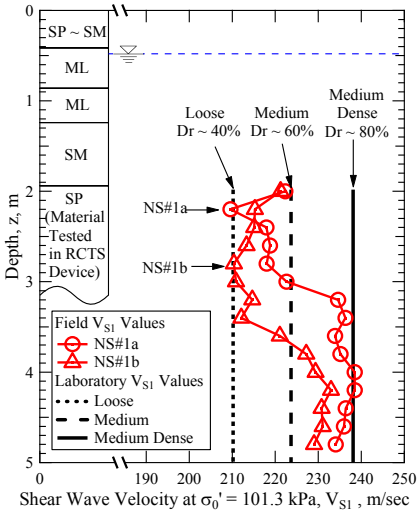


Fig. 5 – Comparison of $V_{S1}$ values from field and lab measurements of liquefiable sand at Site 6

Upon viewing Fig. 4, it is seen that the field $V_S$ profiles in the depth range of 2 to 3.4 m determined at locations NS#1a and NS#1b are generally between the laboratory $V_S$ profiles of sands in the loose ($D_r$ ~ 40%) and medium ($D_r$ ~ 60%) states. This comparison of field and laboratory $V_S$ values indicates that the sand is quite loose in this depth range. In the depth range of about 3.2 to 3.6 m, the field $V_S$ profiles move towards the laboratory $V_S$ profile of the medium-dense sand ($D_r$ ~ 80%). This transition indicates that the sand in this localized zone is becoming somewhat denser with increasing depth. In the depth range of 3.6 to 4.8 m, the field $V_S$ values are in the range between the laboratory $V_S$ profiles of medium ($D_r$ ~ 60%) and medium-dense ($D_r$ ~ 80%) sands. This comparison indicates that the relative density of the sand at this location is increasing with depth. It is important to note, however, that this trend varies around Site 6, and the natural sands are nearly always below the laboratory $V_S$ profile for $D_r$ ~ 80%.

The comparison of the field and laboratory $V_S$ profiles can also be presented in terms of profiles of normalized wave velocities ($V_{S1}$). In this case, $V_S$ values at all depths are adjusted to a confining pressure of 1 atm ($V_{S1} = V_S/(\sigma_0'/P_a)^{ns}$). This comparison is shown in Fig. 5. If the sand skeleton (void ratio) is essential unchanged in the profile and only the confining pressure changes with depth, then the profile of $V_{S1}$ forms a vertical line. In Fig. 5, the $V_{S1}$ profiles from the laboratory data (represented by $D_r$ ~ 40%, ~ 60% and ~ 80%) are vertical lines as expected. On the other hand, this is not true for the field data where considerable variability is seen. There are zones, however, where vertical lines could be reasonably fit the data, such as the depth range of about 3.6 to 4.8 m. Figures 4 and 5 convey the same relative comparison, but Fig. 5 offers an easier way to identify uniform zones.

## 7. Nonlinear Dynamic Properties Determined in the Laboratory

Resonant column (RC) testing over a wide range in $\gamma$ above $\gamma_t^e$ was performed to determine the variations of dynamic properties of the sand specimens in the nonlinear strain range. These tests were performed at three, effective isotropic confining pressures ($\sigma_0$'): 14, 28 and 55 kPa. At each of these low pressures, nonlinear testing was performed after small-strain testing was completed. The results of these measurements at each $\sigma_0$' are presented in terms of variations of shear modulus (G), normalized shear modulus ($G/G_{max}$) and material damping ratio (D) with shear strain ($\gamma$). The strain range was varied from small strains ($\gamma$ < 0.00004%) to strains in the significantly nonlinear range ($\gamma$ ~ 0.1 to 0.2%). The results of the looser specimen from a depth of 2 m are presented as representative of the general trends of all specimens.

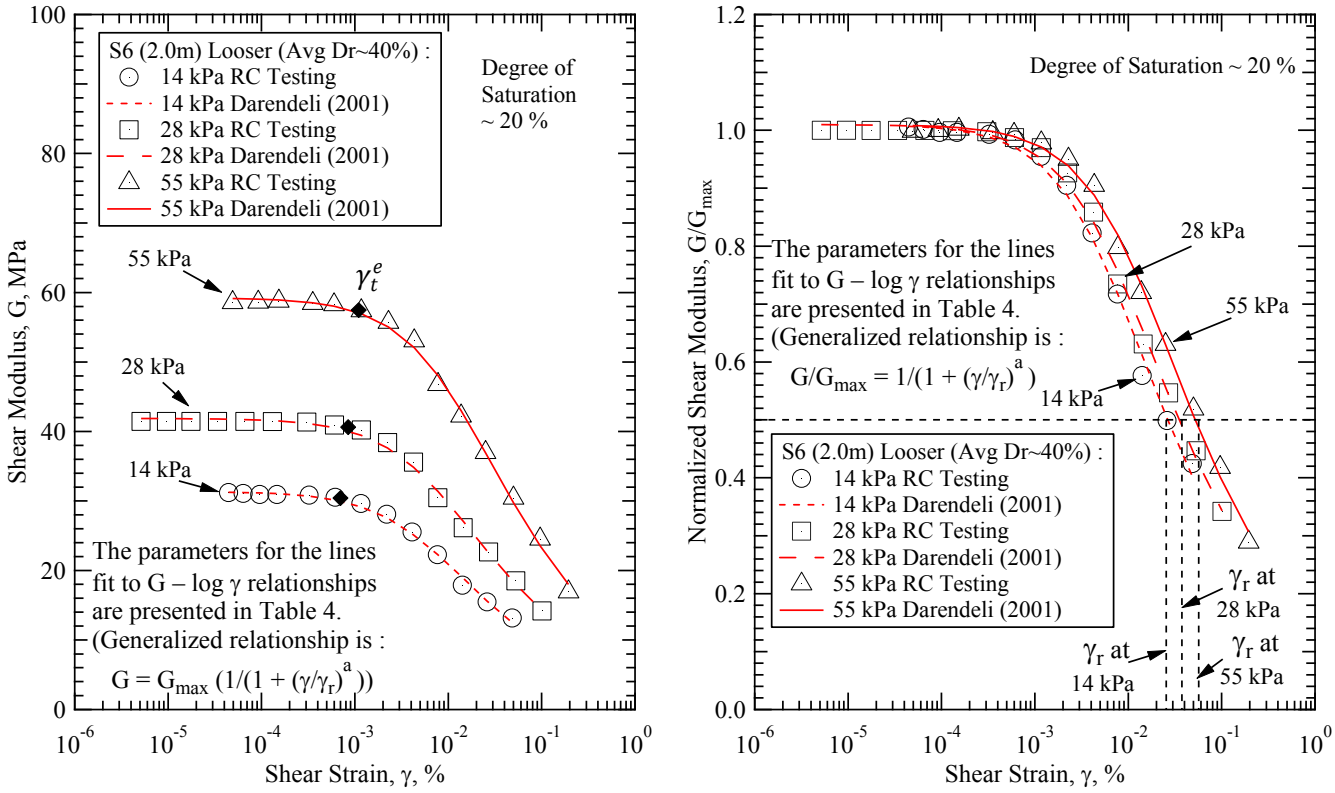


a – Shear modulus reduction curves

b – Normalized shear modulus reduction curves

Fig. 6 –Variations in the G – log γ and G/$G_{max}$ – log γ relationships at values of $\sigma_0$' of 14, 28 and 55 kPa from RC testing of a reconstituted, loose sand specimen from 2 m

The G – log γ relationships at three confining pressures for the looser sand specimen are shown in Fig. 6a. The first point observed is that the value of G at each pressure remains constant when γ is small, and the value of G decreases with increasing γ above the elastic threshold strain, denoted as $\gamma_t^e$. (For ease in identification, $\gamma_t^e$ equals γ at G = 0.98 $G_{max}$.) The second point is that the G – log γ relationships are well represented by a modified hyperbolic equation. The modified hyperbolic equation (Darendeli 2001) [11] used to represent each G – log γ relationship is:

$$G = G_{max}\,(1/(1 + (\gamma/\gamma_r)^a)) \quad (4)$$

in which $G_{max}$ equals the shear modulus in the small-strain range, $\gamma_r$ is equal to the reference strain at which shear modulus equals 0.5 $G_{max}$, and "a" is a curvature coefficient. Each G – log γ relationship has been "best-fit" with Eq. (4) using the least-squares regression method. The resulting best-fit values of the parameters ($\gamma_r$ and "a") are presented in Table 4.

As discussed earlier, $G_{max}$ increases with increasing $\sigma_0$'. Therefore, at a higher value of $\sigma_0$', the nonlinear G – log γ relationship begins at a higher $G_{max}$ value and remains higher with increasing γ, as shown in Fig. 6a. To effectively compare the G – log γ relationships determined at different levels of $\sigma_0$', the shear modulus is normalized by $G_{max}$ at each $\sigma_0$' to form G/$G_{max}$ – log γ relationships. These relationships are plotted in Fig. 6b. Upon comparing the relationships, it is easily seen that the G/$G_{max}$ – log γ relationship translates somewhat to higher shearing strains at higher confining pressures. This translation is captured by values of $\gamma_t^e$ and $\gamma_r$ increasing with increasing $\sigma_0$' as presented in Table 4, with the larger change shown by $\gamma_r$. In Fig. 6b, the strain range where G is constant and equal to $G_{max}$ (hence, G/$G_{max}$ = 1.0) is easily seen at each $\sigma_0$'. This strain range is referred to as the linear, elastic or small-strain range. When shear strain exceeds the elastic threshold strain ($\gamma_t^e$), the normalized shear modulus begins to exhibit nonlinearity. Each specimen has somewhat higher values of $\gamma_t^e$ at

higher $\sigma_0$' as shown in Table 4. As shear strain increases from the linear to moderately nonlinear and then to the significantly nonlinear ranges, the specimen continues to have slightly higher values of $G/G_{max}$ at the same $\gamma$ as $\sigma_0$' increases. As seen in Table 4, for each specimen, values of $\gamma_r$ increase and values of "a" decrease as $\sigma_0$' increases. Further, a linear relationship is found between $\gamma_r$ and normalized pressure ($\sigma_0'/P_a$) with exponent of $n_G$ ($\gamma_r = A_r(\sigma_0'/P_a)^{n_G}$, where $A_r$ is the value of $\gamma_r$ at $\sigma_0$' = 1 atm). These comparisons are true for all specimens.

The variations of material damping ratio with shear strain at the three confining pressures for the looser, sand specimen are shown in Fig. 7. As seen in the figure, values of D at all three confining pressures remain constant when $\gamma$ is small, and increase with increasing $\gamma$. The D – log $\gamma$ relationships can also be represented by a hyperbolic model. The hyperbolic equation used to represent the D – log $\gamma$ relationships is:

$$D/D_{min} = 1 + (\gamma/\gamma_{r,D})^b \quad (5)$$

in which $D_{min}$ equals the material damping ratio in the small-strain range, $\gamma_{r,D}$ is the reference strain at which $D/D_{min}$ equals 2, and "b" is a curvature coefficient. Each D – log $\gamma$ relationship has been "best-fit" with Eq. (5) using the least-squares regression method and the values of $\gamma_{r,D}$ and "b" are presented in Table 5.

Just like the G – log $\gamma$ relationships separated into three different curves (Fig. 6a), the D – log $\gamma$ relationships also separated into three different curves as shown in Fig. 7. However, the difference in the D – log $\gamma$ relationships with $\sigma_0$' is quite small at $\gamma < 0.01\%$. As $\gamma$ increases above 0.01%, the difference in the relationships increases with increasing $\sigma_0$'. It is also interesting to note that D increases more than 10 times over the range in $\gamma$ in the nonlinear RC testing while G only decreases by a factor of about 3. When comparing the D – log $\gamma$ relationships at higher confining pressures, the relationship also translates to higher shearing strains like the $G/G_{max}$ – log $\gamma$ relationships. This translation of the D – log $\gamma$ relationship is captured by values of the variables that identify the reference shear strain in damping, $\gamma_{r,D}$ and the curvature coefficient in damping, "b", at a given $\sigma_0$'. In Fig. 7, it can be seen that the values of $D_{min}$ are very close at the three $\sigma_0$'s when the shear strain is in the small-strain range. As shear strain increases from the linear to moderately nonlinear and then to the significantly nonlinear ranges, the sand specimen exhibits distinctly lower values of D at higher values of $\sigma_0$' (for instance, $\gamma = 0.04\%$). As seen in Table 5, for each specimen, values of $\gamma_{r,D}$ increase and values of "b" decrease as $\sigma_0$' increases. These comparisons are true for all sand specimens tested.

## 8. Impact of Generating Excess Pore Water Pressure on the $G/G_{max}$ – Log $\gamma$ Relationship

It is possible to show the impact of the generation of excess pore water pressure ($\Delta u$) on the shear modulus of the sand at strains above the pore pressure generation threshold ($\gamma_t^{pp}$). The variation of the in-situ pore pressure ratio

Table 4 – Parameters fit to the G – log $\gamma$ relationships determined by RC testing at three confining pressures of reconstituted specimens of looser sand from 2 m and denser sand from 3 m

| Specimen ID. | Effective Confining Pressure, kPa (atm) | Estimated Initial $D_r$[1], % | Void Ratio, e | Elastic Threshold $\gamma_t^e$ [2] (%) | Modified Hyperbolic Relationship[3] | |
|---|---|---|---|---|---|---|
| | | | | | $\gamma_r$ (%) | a |
| S6 (2m) Looser | 14 (0.14) | 40 | 0.784 | 0.0007 | 0.0255 | 0.835 |
| | 28 (0.27) | 40 | 0.783 | 0.00085 | 0.0374 | 0.772 |
| | 55 (0.54) | 40 | 0.781 | 0.0011 | 0.0565 | 0.771 |
| S6 (3m) Denser | 14 (0.14) | 79 | 0.658 | 0.0008 | 0.0315 | 0.851 |
| | 28 (0.27) | 79 | 0.657 | 0.0009 | 0.0380 | 0.778 |
| | 55 (0.54) | 79 | 0.656 | 0.0012 | 0.0562 | 0.777 |

Notes: 1. $D_r = (e_{max} - e)/(e_{max} - e_{min}) \times 100\%$; and $e_{max}$ and $e_{min}$ are average values estimated from Youd (1973) [7] and Menq (2003) [8],
2. $\gamma_t^e$ = shear strain at which $G/G_{max} = 0.98$,
3. modified hyperbolic relationship: $G/G_{max} = 1/(1 + (\gamma/\gamma_r)^a)$.

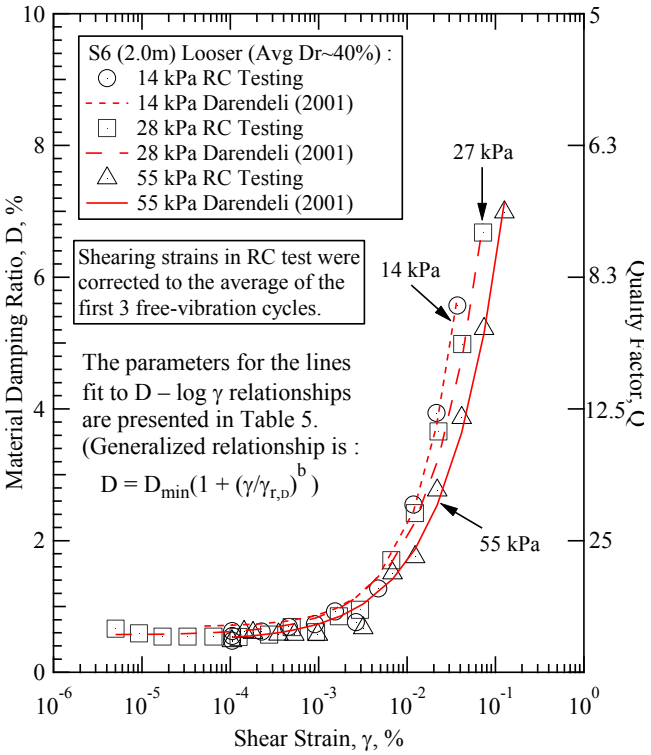


Fig. 7 – Variation in the D – log γ relationships at values of $\sigma_0$' of 14, 28 and 55 kPa

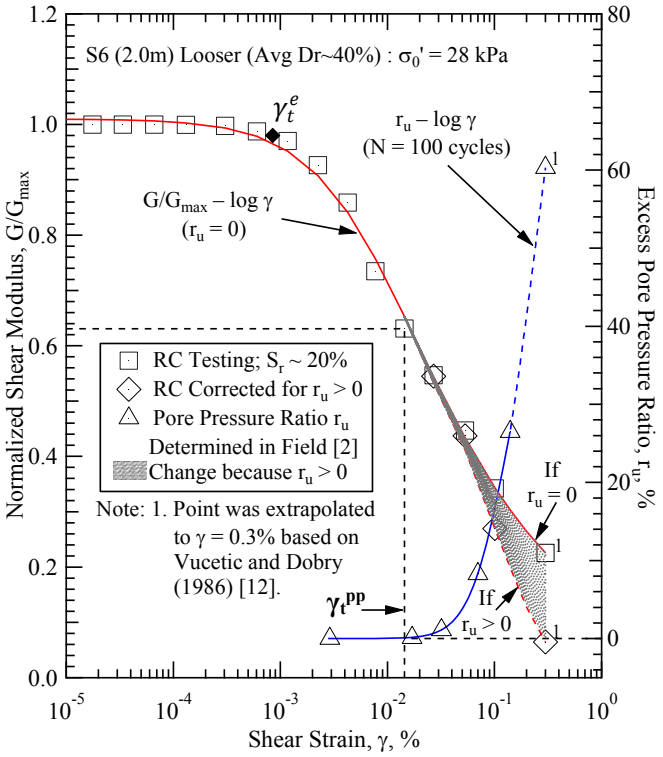


Fig. 8 – Example showing the change in the $G/G_{max}$ – log γ relationship when excess pore pressure is generated

Table 5 – Parameters fit to the D – log γ relationships determined by RC testing at three confining pressures of reconstituted specimens of looser sand from 2 m and denser sand from 3 m

| Specimen ID. | Effective Confining Pressure kPa (atm) | Estimated Initial $D_r$[1], % | Void Ratio, e | Elastic Threshold $\gamma_t^e$[2] (%) | Modified Hyperbolic Relationship[3] | |
|---|---|---|---|---|---|---|
| | | | | | $\gamma_{r,D}$ (%) | b |
| S6 (2m) Looser | 14 (0.14) | 40 | 0.784 | 0.0007 | 0.0024 | 0.832 |
| | 28 (0.27) | 40 | 0.783 | 0.00085 | 0.0026 | 0.726 |
| | 55 (0.54) | 40 | 0.781 | 0.0011 | 0.0037 | 0.699 |
| S6 (3m) Denser | 14 (0.14) | 79 | 0.658 | 0.0008 | 0.0024 | 0.802 |
| | 28 (0.27) | 79 | 0.657 | 0.0009 | 0.0026 | 0.779 |
| | 55 (0.54) | 79 | 0.656 | 0.0012 | 0.0035 | 0.703 |

Notes: 1. $D_r = (e_{max} - e)/(e_{max} - e_{min}) \times 100\%$; and $e_{max}$ and $e_{min}$ are average values estimated from Youd (1973) [7] and Menq (2003) [8],
2. $\gamma_t^e$ = shear strain at which $G/G_{max} = 0.98$
3. modified hyperbolic relationship: $D/D_{min} = 1 + (\gamma/\gamma_{r,D})^b$.

with shear strain ($r_u$ – log γ) determined from field shaking tests at the natural soil site from which these samples were recovered is presented in Fig. 8 (Stokoe et al. 2014) [2]. These measurements were performed at a depth of 2.1 m. Based on the shear wave velocity measured in the field, the looser specimen at $\sigma_0$' of 28 kPa was selected to be representative of the field conditions under which the $r_u$ – log γ relationship was determined. As illustrated in Fig. 8, with increasing γ, $G/G_{max}$ stays constant at 1.0 in the small-strain range and only begins to decrease after $\gamma_t^e$. The value of $r_u$ equals zero in the linear and moderately nonlinear strain ranges, and only begins to increase after the pore pressure generation threshold ($\gamma_t^{pp}$) is reached, which is about 15 times larger than $\gamma_t^e$.

Theoretically, $\gamma_t^{pp}$ is the threshold strain where volume change begins; hence, for $\gamma$ smaller than $\gamma_t^{pp}$, there is no volume change in the soil skeleton. For $\gamma$ larger than $\gamma_t^{pp}$, the tendency of the soil skeleton to densify under shearing generates pore pressure in a saturated sand. As shown in Fig. 8, the value of $\gamma_t^{pp}$ is 0.014%, and the corresponding $G/G_{max}$ value is 0.63. Since $\gamma_t^{pp}$ is the starting point of triggering excess pore pressure ($r_u > 0$), $G/G_{max}$ begins to decrease more rapidly with increasing $\gamma$ for the saturated sand than for the unsaturated sand at $\gamma > 0.014\%$ because of the increasing value of $r_u$ with increasing $\gamma$. The increasing $r_u$ further softens the soil skeleton. This process is termed degradation and occurs in loose saturated sand along with the nonlinearity shown by the unsaturated sand. The modeling of only nonlinearity is represented by Eq. (4). The modeling of both nonlinearity and degradation (Eq. (6)) is discussed below.

Since the degree of saturation of the looser specimen was about 20%, no excess pore water pressure was generated during nonlinear RC testing. Therefore, to simulate the nonlinear field shear modulus reduction curve, the generation of excess pore water pressure needs to be modeled to account for the fully-saturated, field condition. Positive $r_u$ values cause $\sigma_0$' to decrease, which leads to a reduction in G at all strains. Based on Eqs. (2) and (4) and Table 4, the corrected shear modulus reduction curve at any $r_u$ can be represented as:

$$[G/G_{max}]_{cor} = (1 - r_u)^{n_G}/(1 + (\gamma/\tilde{\gamma}_r)^{\tilde{a}}) \quad (6)$$

in which $r_u$ is the excess pore pressure ratio expressed in decimal form, $n_G$ is the stress exponential in the log $G_{max}$ – log $\sigma_0$' relationship, $\tilde{\gamma}_r$ is the $\sigma_0$'-dependent reference strain ($\tilde{\gamma}_r = 0.08((1 - r_u)\sigma_0'/P_a)^{0.57}$ %), and $\tilde{a}$ is the $\sigma_0$'-dependent curvature coefficient ($\tilde{a} = 0.74((1 - r_u)\sigma_0'/P_a)^{-0.06}$). From Fig. 8, it can be seen that for $\gamma$ smaller than $\gamma_t^{pp}$, no correction is made. However, for $\gamma$ larger than $\gamma_t^{pp}$, $G/G_{max}$ is reduced by the correction factor in Eq. (6), and this reduction increases with increasing shearing strain as shown by the darkened zone in Fig. 8. At $\gamma \sim 0.3\%$ for Specimen S6(2.0 m), the value of $G/G_{max}$ has been reduced by a factor of 3 (to a value of $G/G_{max} \sim 0.07$) by the increased pore pressure as seen in Fig. 8.

## 9. Summary and Conclusions

Torsional resonant column tests were performed to study the small-strain and nonlinear dynamic properties of liquefiable sand from Christchurch, NZ. The sand classifies as a poorly graded sand (SP) and has less than 3% fines. For the small-strain dynamic properties, $V_S$, $G_{max}$ and $D_{min}$ form linear relationships with $\sigma_0$' on a log-log scale, with $V_S$ and $G_{max}$ increasing with increasing $\sigma_0$' and $D_{min}$ decreasing with increasing $\sigma_0$'. Void ratio (e) has a modest influence on the log $V_S$ – log $\sigma_0$' and log $G_{max}$ – log $\sigma_0$' relationships in the general way that denser soils form stiffer soil skeletons. Void ratio has a small influence on the log $D_{min}$ – log $\sigma_0$' relationship, with denser specimens exhibiting slightly smaller $D_{min}$ values than looser specimens at the same $\sigma_0$'.

The small-strain $G_{max}$ values of the liquefiable sand determined from RC testing in this study are also compared with earlier laboratory RC measurements of soft soils that liquefied in earthquakes in Imperial Valley, California. The log $G_{max}$ – log $\sigma_0$' relationships of the specimens from California compare well with the relationships for the loose Christchurch sands. However, the Imperial Valley soils are somewhat denser and have significantly more fines (SM and SP-SM materials). These two factors seem to combine to counteract each other, resulting in soft, liquefiable silty soils. Laboratory $V_S$ profiles of the sand in Christchurch are also compared with results from field crosshole testing. This comparison indicates that $D_r$ of the sand at this location is variable, sometimes increasing with depth and sometimes decreasing over the depth range of about 2 to 5 m. The looser sand falls in the $D_r$ range of 40 to 60% and the denser sand falls in the range of 60 to 80%.

For the nonlinear dynamic properties of the unsaturated sand tested, both the G – log $\gamma$ and D – log $\gamma$ relationships can be represented by modified hyperbolic models, with G decreasing and D increasing with increasing $\gamma$ in the nonlinear range. Confining pressure has an influence on the nonlinear shear modulus behavior, with values of $\gamma_t^e$ and $\gamma_r$ increasing and values of "a" decreasing as $\sigma_0$' increases. The magnitude of $\sigma_0$' also has an influence on the nonlinear material damping behavior, with values of $\gamma_{r,D}$ increasing and values of "b" decreasing as $\sigma_0$' increases. This behavior represents nonlinearity in the unsaturated sand.

To account for the fully saturated condition of the sand in Christchurch, the generation of excess pore pressure has to be modeled to determine the nonlinear field shear modulus reduction curve. Positive $r_u$ causes $\sigma_0$'

to decrease, which leads to a reduction in shear modulus from both nonlinearity and degradation. A new equation, Eq. (6), was formulated to model the combined processes. The results of modeling both processes are shown in Fig. 8 as is the threshold for pore pressure generation, $\gamma_t^{pp}$, evaluated during field testing [2].

## 10. Acknowledgements

Partial financial support for this study was provided through the National Science Foundation under a grant from the RAPID program (CMMI–1343524) and from the New Zealand Earthquake Commission (EQC). Thanks also goes to graduate students and staff at the University of Texas at Austin including Ms. Julia Roberts, Mr. Boonam Shin, Mr. Sungmoon Hwang, Prof. Brady Cox and Dr. Farn-Yuh Menq.

## 11. Copyrights



## 12. References

[1] Van Ballegooy S, Wentz F, Stokoe K, Cox B, Rollins K, Ashford S, Olsen M (2017): Christchurch Ground Improvement Trial Report. *Report for the New Zealand Earthquake Commission.* (In press).

[2] Stokoe KH, Roberts JN, Hwang S, Cox BR, Menq FY, Van Ballegooy S (2014): Effectiveness of inhibiting liquefaction triggering by shallow ground improvement methods: Initial field shaking trials with T-Rex at one site in Christchurch, New Zealand. *Soil Liquefaction during Recent Large-Scale Earthquakes – Orense, Towhata & Chouw (Eds),* pp. 193-202, Taylor & Francis Group, London, ISBN 978-1-138-02643-8.

[3] Richart FE, Hall JR, Woods RD (1970): *Vibrations of soils and foundations*. Prentice-Hall, 414 p.

[4] Keene AK (2017): Next-generation equipment and procedures for combined resonant column and torsional shear testing. *Ph.D. Dissertation*, The University of Texas at Austin (in progress).

[5] ASTM Standard D6913-04 (2009): Standard test methods for particle-size distribution (gradation) of soils using sieve analysis. *American Society for Testing of Materials ASTM International*, West Conshohocken, Pennsylvania, USA, DOI: 10.1520/D6913-04R09E01.

[6] ASTM Standard D2487-11 (2011): Standard practice for classification of soils for engineering purposes (Unified Soil Classification System). *American Society for Testing of Materials ASTM International*, West Conshohocken, Pennsylvania, USA, DOI: 10.1520/D2487-11.

[7] Youd TL (1973): Factors controlling maximum and minimum densities of sands. *ASTM STP* 523, pp. 98-112.

[8] Menq FY (2003): Dynamic properties of sandy and gravelly soils. *Ph.D. Dissertation*, The University of Texas at Austin, 364 p.

[9] Ladd RS (1978): Preparing test specimens using undercompaction. *Geotechnical Testing Journal*, GTJODJ, Vol. 1, No. 1, pp. 16-23.

[10] Hardin BO (1978): The nature of stress-strain behavior of soils. *Earthquake Engineering and Soil Dynamics, ASCE,* Vol. 1, pp. 3-90.

[11] Darendeli BM (2001): Development of a new family of normalized modulus reduction and material damping curves. *Ph. D. Dissertation*, The University of Texas at Austin, 362 p.

[12] Vucetic, M, Dobry, R (1986): Pore Pressure Build Up and Liquefaction at Level Sandy Sites During Earthquakes. *Research Report*. Department of Civil Engineering at Rensselaer Polytechnic Institute, Troy, USA.

[13] Kuo HJ (1982): Static and dynamic properties of sands subjected to 1979 Imperial Valley Earthquake. *M.S. Thesis*, The University of Texas at Austin, 268 p.

[14] Haag ED (1985): Laboratory investigation of static and dynamic properties of sandy soils subjected to the 1981 Westmorland Earthquake. *M.S. Thesis*, The University of Texas at Austin, 247 p.